CrossMark

Ability of High-Resolution Resistivity Tomography to Detect Fault and Fracture Zones: Application to the Tournemire Experimental Platform, France

C. Gélis,[1] M. Noble,[2] J. Cabrera,[1] S. Penz,[2] H. Chauris,[2] and E. M. Cushing[1]

Abstract—The Experimental Platform of Tournemire (Aveyron, France) developed by IRSN (French Institute for Radiological Protection and Nuclear Safety) is composed of a tunnel excavated in an argillite formation belonging to a limestone–argillite–limestone subhorizontal sedimentary sequence. Subvertical secondary fault zones were intercepted in argillite using drifts and boreholes in the tunnel excavated at a depth of about 250 m located under the Larzac Plateau. A 2D 2.5 km baseline large-scale electrical resistivity survey conducted in 2007 allowed detecting in the upper limestones several significantly low electrical resistivity subvertical zones (GÉLIS *et al*. Appl Geophys 167(11): 1405–1418, 2010). One of these discontinuities is consistent with the extension towards the surface of the secondary fault zones identified in the argillite formation from the tunnel. In an attempt to better characterize this zone, IRSN and MINES ParisTech conducted a high-resolution electrical resistivity survey located transversally to the fault and fracture zones. A 760-m-long profile was acquired using two array geometries and take-outs of 2, 4 and 8 m, requiring several rollalongs. These data were first inverted independently for each takeout and then using all take-outs together for a given array geometry. Different inverted 2D electrical resistivity models display the same global features with high (higher than 5000 Ωm) to low (lower than 100 Ωm) electrical resistivity zones. These electrical resistivity models are finally compared with a geological cross-section based on independent data. The subvertical conductive zones are in agreement with the fault and fracture locations inferred from the geological cross-section. Moreover, the top of a more conductive zone, below a high electrical conductive zone and between two subvertical fault zones, is located in a more sandy and argillaceous layer. This conductive zone is interpreted as the presence of a more scattered fracture zone located at depth between two fault zones. This zone could be correlated with the fractured zones identified at 250-m depth in underground works. This study highlights the interest of multi-scale approaches to image complex heterogeneous near subsurface layers. Finally, this study shows that the electrical resistivity tomography is a useful and powerful tool to detect fault and fracture zones in upper limestones. Such a method is complementary to other geophysical and geological data.

1. Introduction

Deep argillaceous formations are considered in many countries as potential host media for high-level long-life radioactive waste due to their physical properties, such as their very low intrinsic permeability and their strong capacity for radionuclide retention (LEROY *et al*. 2007; YVEN *et al*. 2007). The sedimentary and structural characterization of such potential host sites is a key point to determine their ability as being safe for the long-term deep underground disposal of radioactive waste in a geological formation (BONIN 1998; BOISSON *et al*. 2001). Examples include the Callovo-Oxfordian formation of the Paris basin for instance (TROUILLER 2006). The presence of secondary faults in argillaceous formations (or argillite) must be particularly well assessed since they could change various argillite properties such as permeability. Such faults are expected to be extremely scattered and may display small vertical offsets due to the subhorizontal displacement during the tectonic events. The site characterization and fracture detection can be performed using complementary approaches. They include geological and tectonic studies in analogue sites, in situ investigations with boreholes, and non-destructive geophysical methods to image such argillaceous formations from the ground surface.

IRSN (the French Institute for Radiological Protection and Nuclear Safety) is involved in the safety analysis of reports of the French deep geological disposal project in the Meuse/haute-Marne site. This

[1] PRP-DGE Department, Institute for Radiological Protection and Nuclear Safety, Fontenay-Aux-Roses, France. E-mail: celine.gelis@irsn.fr
[2] Centre de Géosciences, MINES ParisTech, Fontainebleau, France.

site will be operated by ANDRA (the French Radioactive Waste Management Agency). With the goal of understanding the various transport and mechanical properties of argillite, IRSN has conducted a wide range of experiments at the Tournemire Experimental Platform (Aveyron in the south of France) (see e.g., Bonin 1998; Boisson et al. 2001). In this site, secondary fault zones such as those previously mentioned have been observed in an underground tunnel. They have also been identified in boreholes and galleries that were drilled from the tunnel. Field observations are consistent with the hypothesis of an upward extension of these scattered faults to the surface.

Because of its sensitivity to water and argillite content, electrical resistivity tomography (ERT) is currently considered as an efficient tool to delineate fractures and karstified zones characterized by low electrical resistivity (ER) values. This method has proven to be very useful in many studies such as environmental issues (e.g., Frid et al. 2008; Hamzah et al. 2006; Guérin et al. 2004), landslides and rock-slides study and monitoring (e.g., Meric et al. 2005; Grandjean et al. 2009), basin geological and structural characterization (e.g., Rizzo et al. 2004), fault detection in subsurface layers (e.g., Suzuki et al. 2000; Demanet et al. 2001; Nguyen et al. 2007; Vanneste et al. 2008; Improta et al. 2010) and preferential flow pathway in fractured and karstified limestones (e.g., Robert et al. 2011). ERT survey has been mainly used for small-scale studies (even centimeter scale for excavation damaged zone monitoring, e.g., Kruschwitz and Yaramanci 2004; Gibert et al. 2006). This method can also be applied at the scale of several kilometers (Storz et al. 2000; Revil et al. 2008). For a review of the ERT method, the reader is invited to refer to Binley and Kemna (2005).

Nguyen et al. (2005, 2007) give a critical overview of the difficulties encountered when using the ERT method to image complex structures. They stress that ERT results provide an electrical resistivity image that has to be carefully interpreted when using inversion software such as the Res2DInv of Loke and Barker (1995). Nguyen et al. (2005) pointed out that the resulting image could be highly influenced by the inversion scheme itself and by the very strong hypotheses that the inverse scheme is formulated as a locally linear problem. They also highlight the difficulty of precisely delineating the position of boundaries between different zones.

To assess the potential of ERT to image faults and fracture zones in the Tournemire Experimental Platform, Gélis et al. (2010) applied the Res2DInv software to electrical resistivity data acquired with a large take-out (40 m). They were able to image the argillaceous layer that appears as an almost homogeneous conductive layer. The authors found that in the upper limestone layer overlaying the argillaceous layer, electrical resistivity values are strongly heterogeneous and range from 100 to 5000 Ωm. In particular, they identify a conductive zone that could correspond to an upward continuation of fault zones identified from underground works. However, the large electrode spacing did not allow them to infer precisely the geometry of this zone, especially near the subsurface where the soil appeared to be highly heterogeneous.

In an attempt to address this problem, IRSN and MINES ParisTech conducted a high-resolution electrical resistivity survey to evaluate the potential of ERT to finely image fault and facture zones in upper limestones. The term "high resolution" was chosen to emphasize the electrode spacing differences between this new acquisition and the first one. Measurements were performed with several electrode take-outs (2, 4 and 8-m) and two acquisition geometries to appraise their influence on ERT results and to assess the benefit of a high-resolution multi-scale approach. 1D vertical and horizontal profiles are also extracted from ERT images obtained with the different acquisitions geometries and surveys and are compared quantitatively for different horizontal distances and at different depths. This allows to assess the coherency between the large-scale and the high-resolution surveys. Finally, ERT results are interpreted with the help of a geological cross-section. This study highlights the interest of a multi-scale approach to image the complex heterogeneous near subsurface medium.

This paper is divided into four main sections. After presenting the geological context of the Tournemire Experimental Platform in Sect. 2, the main results of the 2007 2.5 km baseline large-scale Electrical Resistivity tomography (ERT) survey are summarized in Sect. 3. Section 4 is dedicated to the

new high-resolution ERT survey. This survey is a 760-m-long line where the data are acquired for two distinct geometry arrays and three different take-outs. 2D ERT models obtained with individual or all take-outs are compared for a given acquisition scheme (Wenner or Schlumberger). These models are finally interpreted and compared with a geological cross-section built from independent data in Sect. 5.

2. The Tournemire Experimental Platform: Geological Context

From a regional point of view, the Tournemire experimental platform is located in a Mesozoic marine basin on the southern border of the French Massif Central. The sedimentary series are characterized by three major subhorizontal units (BONIN 1998; BOISSON *et al.* 1996). From top to bottom, we first find (1) a sequence of limestone and dolomite layers (50- to 120-m-thick Bathonian, around 150-m-thick Bajocian, and 15- to 20-m-thick Upper Aalenian) (see Fig. 1). It is worth mentioning that these Bathonian and Bajocian formations are locally karstified. They overlie a (2) 250-m-thick argillite layer of Toarcian and Domerian age. Under this argillaceous formation, we find a sequence of (3) limestone and dolomite Carixian and Sinemurian layers.

Tectonic evolution appears first characterized by an extensional tectonic event. During Hettangian-Sinemurian times (Lower Lias), an east–west trending extension initially occurred, progressively changed to NW–SE near the Sinemurian-Carixian limit. This NW-trending extension continued until Middle-Jurassic time when a north-trending extension occurred. Normal faults, east–west oriented, were then created or reactivated. One of these faults is the Cernon Fault, which is the main regional fault located at the Tournemire Experimental Platform (Figs. 1, 2). The north-trending extension lasted until Late Jurassic. During the late Cretaceous and Eocene times, the Pyrenean tectonics was responsible for a general compressional stress field in the Eurasian plate. Inherited structures, such as the Cernon fault, were reactivated as reverse or strike–slip faults, whereas other faults were created with reverse or strike–slip kinematics. The Oligocene–early Miocene extension occurring in the south-east of France did not affect the studied area. No evidence of Plio-Quaternary tectonic activity has been reported in the region, but some relics of tiny local volcanoes (spread on N-S trending direction) can be observed only few kilometers westwards.

The Tournemire Experimental Platform was chosen by IRSN because the thick Toarcian and Domerian argillite layer was thought to be a good analogue of the Calloxo-Oxfordian clay-rock found in the Paris basin where is located the underground laboratory of ANDRA. This site is also characterized by a more than 100-year-old 2-km-long railway
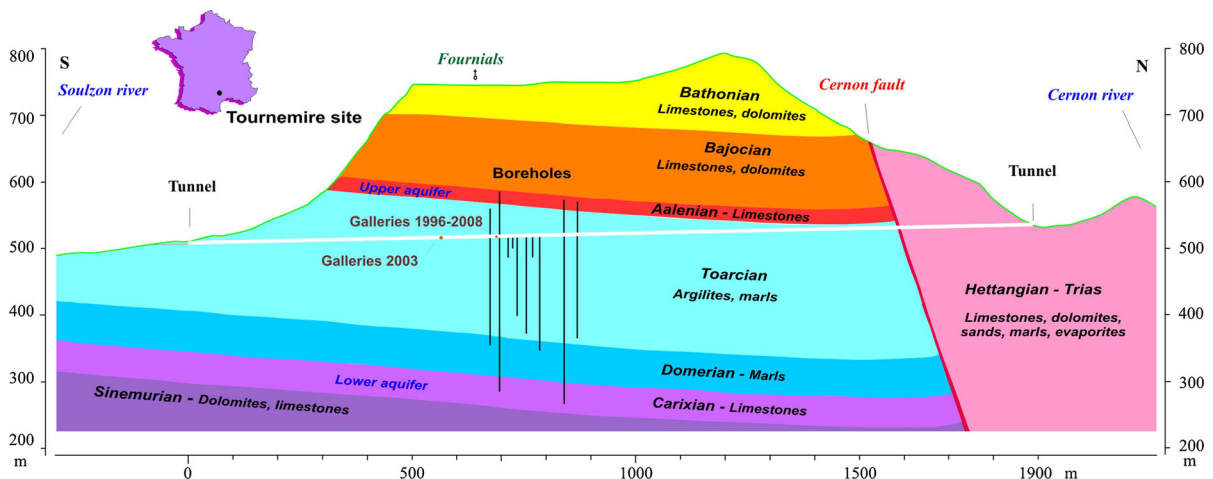

Figure 1
North–south oriented geological cross-section of the Tournemire plateau. The experimental platform is located in the central part of the tunnel
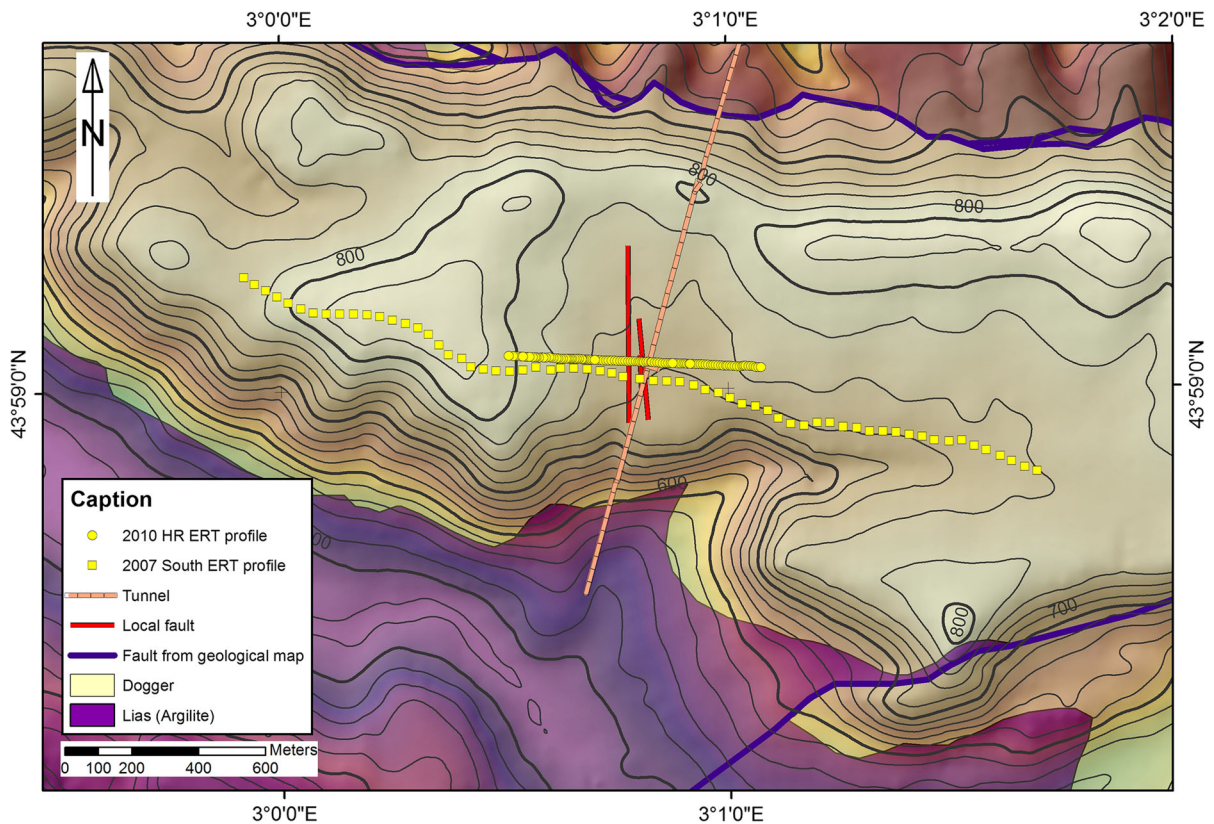
Figure 2

Geological map of the Tournemire plateau showing the position of the tunnel and the position of the 2007 and 2011 electrical resistivity profiles. The east–west regional Cernon fault (*dark blue line*) crosses the tunnel in its northern part. The *red lines* indicate the secondary fault zone identified in the tunnel in the argillaceous formation. These faults are oriented along a north–south trend

tunnel, which allows an in situ access to the Toarcian argillite layer (Fig. 1). IRSN drilled several drifts and many boreholes from this tunnel.

In addition to the main Cernon fault, secondary fault zones affect the argillaceous formation and are directly observed from underground works (BONIN 1998; CABRERA *et al.* 2001). These hectometer-long subvertical faults or network of fractures display a throw of several meters and a larger heave (around 10–15 m). They present also significant variations in their aspect, from a fault gouge (approximately 1 m wide) to a breccia associated with a wider fractured zone (between 10 and 20 m) (CABRERA *et al.* 2001). These strike–slip fractures are roughly N–S oriented and were created or reactivated during the Pyrenean tectonic phase. Their location is reported in Fig. 2.

These secondary faults just mentioned were intercepted in the argillite from drifts and boreholes drilled from the tunnel at a depth of about 250 m. In

the upper limestone, these fault zones are supposed to widen as fractures become more scattered. Field observations tend to confirm this hypothesis and even suggest that these scattered faults might even extend right up to the surface.

In this geological context, the objective of this study presented in this paper is to assess the potential of ERT to detect such faults from surface measurements. In the next section, we will summarize the main results from a previous large-scale ERT survey acquired in 2007 on this experimental platform (GÉLIS *et al.*, 2010).

3. Large-Scale 2007 ERT Acquisition

A large-scale electrical resistivity survey test was conducted in 2007 at the Tournemire experimental platform from the surface by IRSN in

collaboration with the CNRS. In this section, we focus only on the main results of this experiment. For further details, the reader is invited to refer to GÉLIS *et al*. (2010).

During this survey several profiles were acquired, only results for the south NNW–SSE line that is roughly perpendicular to the secondary fault zones described in the previous section is presented. The geographical location of this line with respect to the secondary fault zones that we expect to image is shown in Fig. 2. A 2520-m-long cable was used with a take-out of 40 m and 64 electrodes. Measurements were performed with a Wenner-alpha array. The apparent resistivity measurements were used as observed data to perform an inversion with the Res2DInv software (LOKE and BARKER 1995, 1996). Several tests regarding the inversion type (data and model norms choice) were performed. The Occam–Marquardt inversion was finally chosen because it seemed to better handle the presence of strong electrical resistivity contrasts observed in the data.

The final interpretation of this south profile is shown in Fig. 3. The distribution of low and high electrical resistivity zones shows well-contrasted resistivity bodies that can be interpreted as the signature of geological layers of the site. The argillite layer (labeled Toarcian in Fig. 3) is identified at the bottom of the resistivity image, with electrical resistivity values ranging from 90 to 150 Ωm. These values in terms of resistivity are in agreement with measurements made in laboratory on argillite borehole samples (COSENZA *et al*. 2007).

The lateral electrical resistivity contrasts observed essentially in the two upper layers (Bathonian and Bajocian limestones and dolomites) are interpreted as the signature of faults. It must be noted that due to the low resolution resulting from the large electrode spacing (40 m), location of these faults is not very accurate. As a consequence, the approximate locations of faults are indicated on each profile with dotted lines. Faults were plotted with a vertical dip to avoid an over-interpretation of the shape of the lateral resistivity contrasts.

The top layer (30–150 m thick) corresponds to the karstified Bathonian limestone and dolomite. Its relatively low electrical resistivity in some areas (200–600 Ωm) is interpreted as fracturing. Fracturing has been observed on the side of the plateau and is spatially heterogeneously distributed. Below, a generally more electrically resistive layer is identified on the ERT image. The resistivity of this layer (Bajocian limestone and dolomite) is not homogeneous along the profile and is interpreted as degrees of fracturation that varies in space. High electrical resistivity values, around 4000 Ωm, correspond to unfractured limestone and smaller resistivity values, around 800–1500 Ωm, are interpreted as fractured limestone.

Discussing more in detail the different signatures of faults observed in the ERT image, we first observe at 420 m distance from the origin point along the profile (F3 in Fig. 3) a more electrically conductive fractured zone that affects the Bajocian limestone (roughly 800 Ωm with respect to surrounding electrical resistivity equal to 3000 Ωm). This electrical
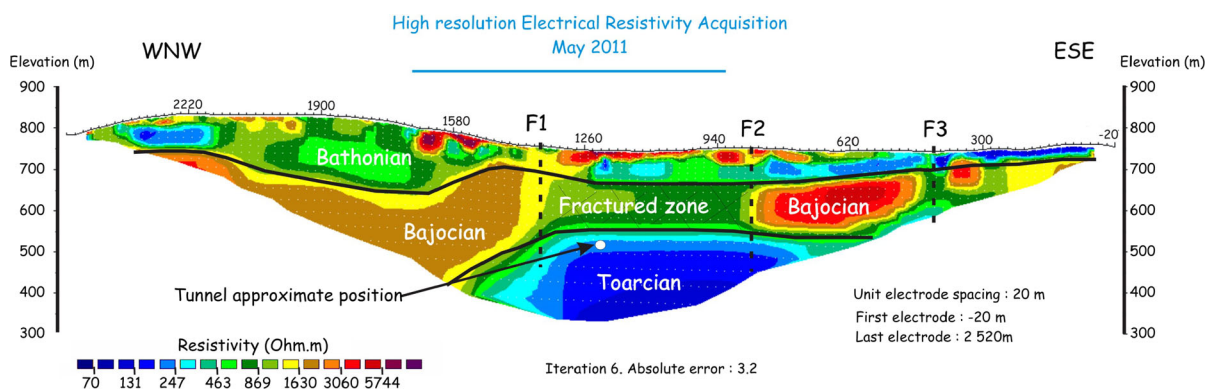

Figure 3
Interpreted electrical resistivity tomography image of the 2007 large-scale acquisition, modified from GELIS *et al*. (2010). The *blue line* indicates the position of the 2011 high-resolution survey

resistivity contrast is interpreted by the authors as an indication of the presence of a fault. A large electrically conductive zone (around 600–1200 Ωm) can be observed from 860 to 1340 m from the beginning of the profile. These zones are attributed to faulted material (F1 and F2 in Fig. 3). The fault zone identified around at 1340 m (F1) may correspond to the extension towards the surface of the almost N–S-trending subvertical fault zones observed inside the tunnel (CABRERA et al. 2001) (Fig. 2).

This profile acquired with a 40-m electrode spacing did enable to image the subsurface down to a depth of approximately 250–300 m. This same electrode spacing prevented us from obtaining a high-resolution image. In an attempt to characterize in more detail the lower resistivity fractured zone in the upper limestones and dolomites layer, we conducted a high-resolution (HR) ER acquisition in May 2011. This survey is described in the next section.

4. High-Resolution Electrical Resistivity Tomography

In order to better understand the relation between fault zones observed in the underground works and fractured zone in the upper limestones and dolomites, IRSN and MINES ParisTech performed a high-resolution profile on the same area using a smaller electrode spacing. This survey was centered on the western part of the fractured zone in the Bajocian and Bathonian limestones and dolomites above the tunnel (Figs. 2, 3). We present in this section the data acquisition and electrical resistivity tomography images obtained from these data. We then compare these high-resolution ERT images with the large-scale ones obtained in 2007.

4.1. High-Resolution Electrical Resistivity Surveys

A 760-m-long profile was successively sampled with 8 and 4 m electrode spacing. In addition two-thirds of this profile (510 m in the central part) was acquired with a 2-m electrode spacing. Measurements were performed with a 64 electrode multi-channel (12) Abem Terrameter acquisition system, requiring for each profile several roll-alongs. For each

electrode spacing, measurements were successively performed along the profile with Wenner-alpha and Schlumberger arrays. Wenner array was chosen in order to compare high-resolution ERT results with large-scale ones obtained with the Wenner array. This array is mainly sensitive to horizontal structures. However, as shown by DAHLIN and LOKE (1998), this array is able to image vertical structures provided that the Gauss–Newton inversion is chosen as inversion method. The Schlumberger array was tested because it is sensitive to both horizontal and vertical structures. DAHLIN and ZHOU (2004) show the capacity of these two arrays to image a conductive dike embedded in a resistive layer. Comparing ERT images obtained with these two arrays allows to assess their impact on electrical resistivity images.

On the whole, these data are of high quality. The variation coefficient of the output voltage is lower than 1 % for 99 % of the data for 4 m arrays, for 98 and 94 % for the 8 m Wenner and Schlumberger arrays, respectively. For the 2-m arrays, the western part of the profile presents a higher variation coefficient due to a lower output voltage.

The apparent resistivity measurements are used as observed data to perform an inversion with the Res2DInv software (LOKE and BARKER 1995, 1996). The surface topography along the profile does exhibit relatively strong variations and was carefully measured on the field and taken into account in the inversion. We perform several tests using different kinds of inversion norms (for the data misfit and model constraints). The distributions of low and high electrical resistivity zones remain similar, but maximum inverted electrical resistivity values were different. Since high electrical resistivity contrasts are present in this area and in order to be consistent with the large-scale electrical resistivity data processing, observed data were inverted with the Marquardt–Occam inversion method following GÉLIS et al. (2010). The maximum number of iterations was set to 5 in order to get main electrical resistivity zones and to avoid over-interpreting data in such complex zones. Further iterations did not globally improve the images.

Figure 4 shows the ERT profiles for the three electrode spacings (8, 4 and 2 m) and the two acquisition arrays (Wenner and Schlumberger). To

compare the different electrical resistivity models, the vertical scale is equal to twice the horizontal scale and the color scale is the same for each ERT model.

Figure 5 shows observed and calculated apparent electrical resistivities for the two arrays and the three different electrode spacings. The match between the observed and the calculated data is generally good and for all inversions, the final RMS values are lower than 8 %.

The Schlumberger 8-m electrode spacing profile penetrates down to a depth of approximately 100 m. The section shows highly contrasted areas with resistivity values ranging from 200 Ωm (and even lower) to 5000 Ωm. On the whole, the 8-m electrode spacing Wenner array displays the same low-to-high electrical resistivity zones and the values are comparable to the Schlumberger 8-m array. This is fairly logical in the sense that Schlumberger and Wenner electrode geometries are similar.

When the electrode spacing decreases, the maximum investigated depth also decreases as the number of electrodes used for the measurements is constant, but lateral and vertical resolution increases. Electrical resistivity sections generally display the same low-to-high electrical resistivity zones whatever the electrode spacing and acquisition array (Fig. 4). This indicates that electrical resistivity images are stable. Superimposed 1D vertical and horizontal profiles for different arrays and electrode spacings show quantitatively the stability of the results (Figs. 6, 7). CAPUTO et al. (2003) also observed similar stability when trying to image across a fault with varying electrode spacing. The resolution and accuracy of electrical resistivity images are expected to decrease with depth. Since electrical resistivity images obtained with all electrode spacings are globally comparable, this suggests that we can trust images obtained with 2 and 4 m electrode spacings until their maximum depths (Figs. 4, 6, 7). This is confirmed by the relative sensitivity matrix values. Following ROBERT et al. (2011), we use a cut-off value of 0.1 (10 %) to assess the reliability of ERT images. Apart from isolated points, one main zone with relative sensitivity values lower than 0.1 appears
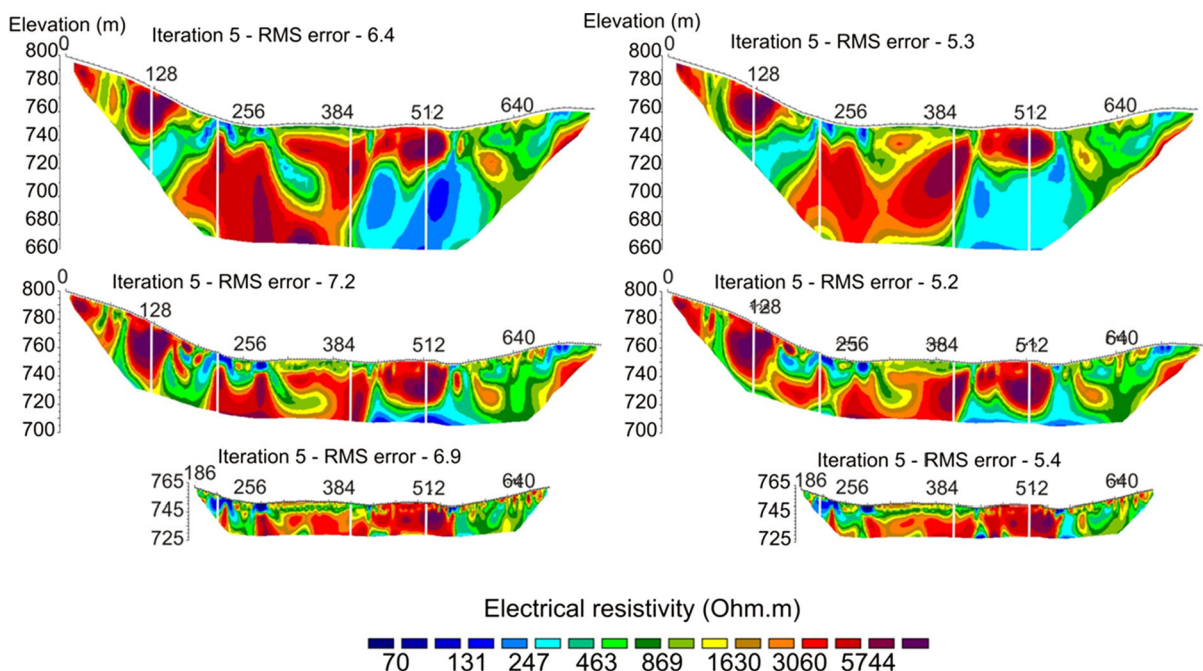

Figure 4

Electrical resistivity tomography images of the 2011 high-resolution acquisition. The results are displayed in the *left column* for the Schlumberger array and in the right column for the Wenner array. From *top* to *bottom*, the images corresponds to the 8, 4 and 2 m electrode spacing. All sections are displayed with the same color scale; Fig. 3 is also displayed with the same scale. Vertical scale is equal to twice the horizontal scale. *White vertical lines* indicate the position of 1D profiles displayed in Fig. 6
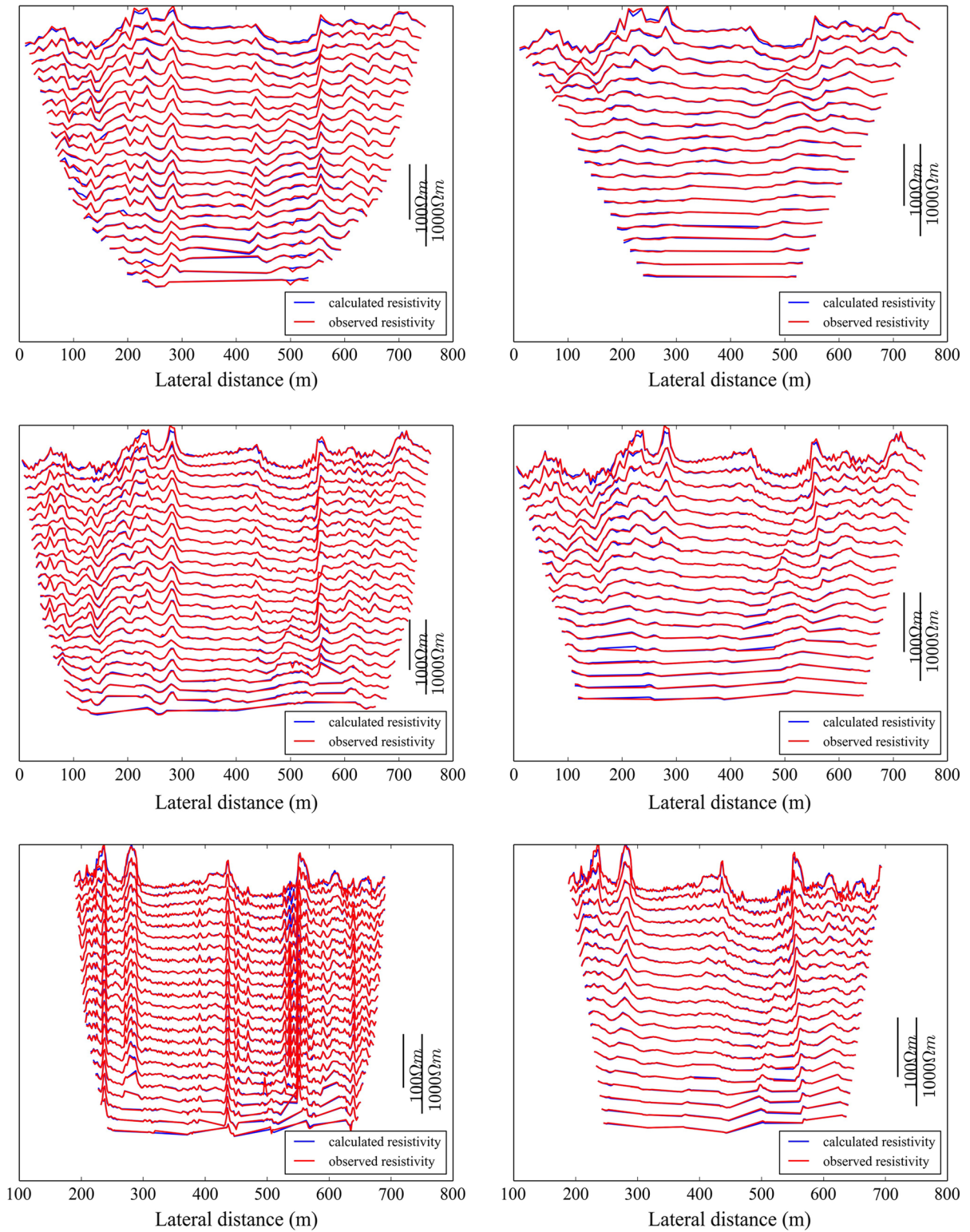
Figure 5

Observed (*red*) and calculated (*blue*) apparent electrical resistivity profiles for the two arrays and the three different electrode spacings corresponding to the sections displayed in Fig. 4
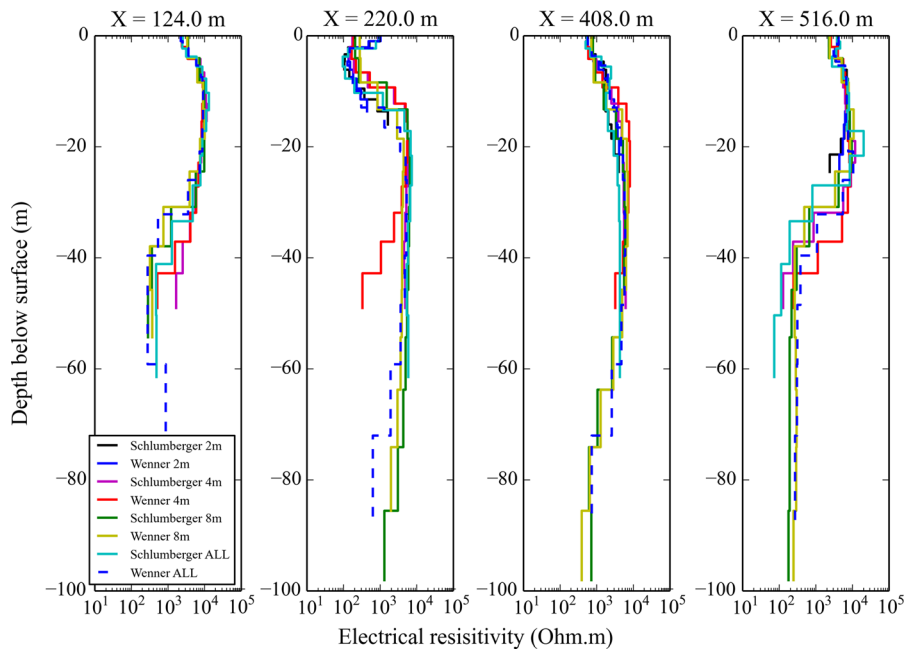
Figure 6
1D vertical electrical resistivity profiles extracted from the 2D high-resolution sections at different lateral positions (from *left* to *right*: 124, 220, 408 and 516 m)
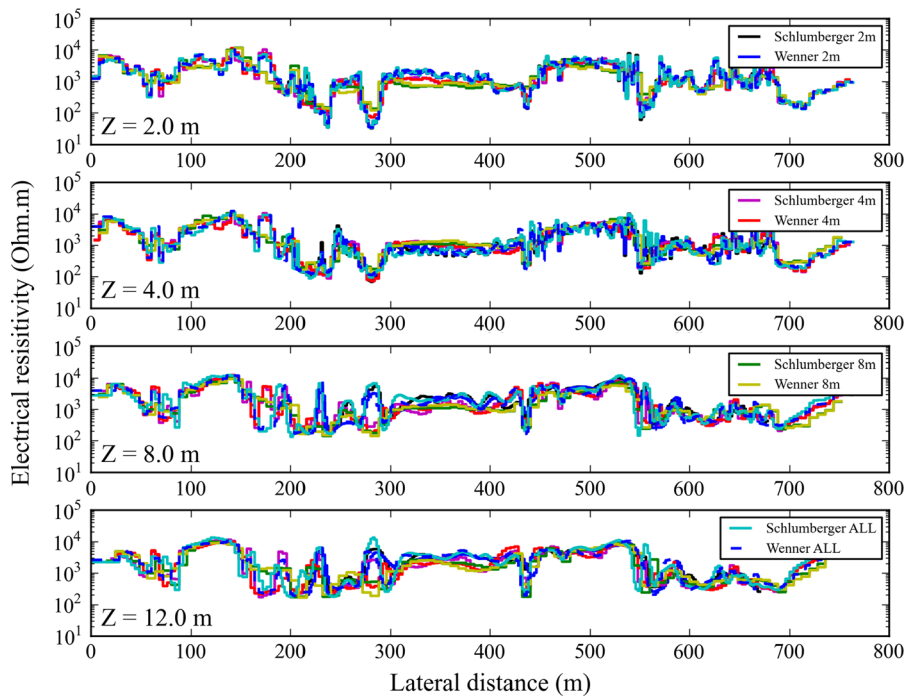

Figure 7
1D horizontal electrical resistivity profiles extracted from the 2D high-resolution sections at increasing depth below topography (from *top* to *bottom*: 2, 4, 8 and 12 m). The *different colors* correspond to the different acquisitions (see *legends*)
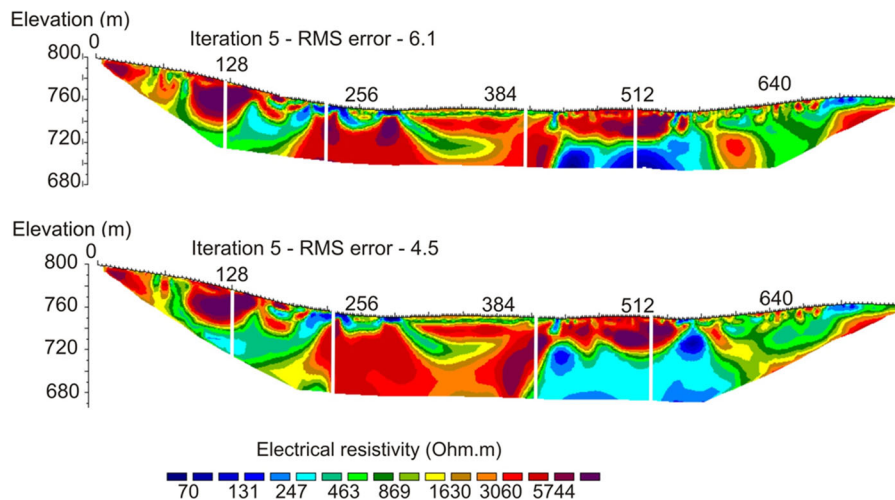
Figure 8
Electrical resistivity tomography images of the 2011 high-resolution acquisition combining together all electrode spacing data (2, 4 and 8 m). *Top* corresponds to the Schlumberger array, and *bottom* to the Wenner array. These sections are displayed with the same color scale as Figs. 3 and 4. Vertical scale is equal to horizontal scale. *White vertical lines* indicate the position of 1D profiles displayed in Fig. 6
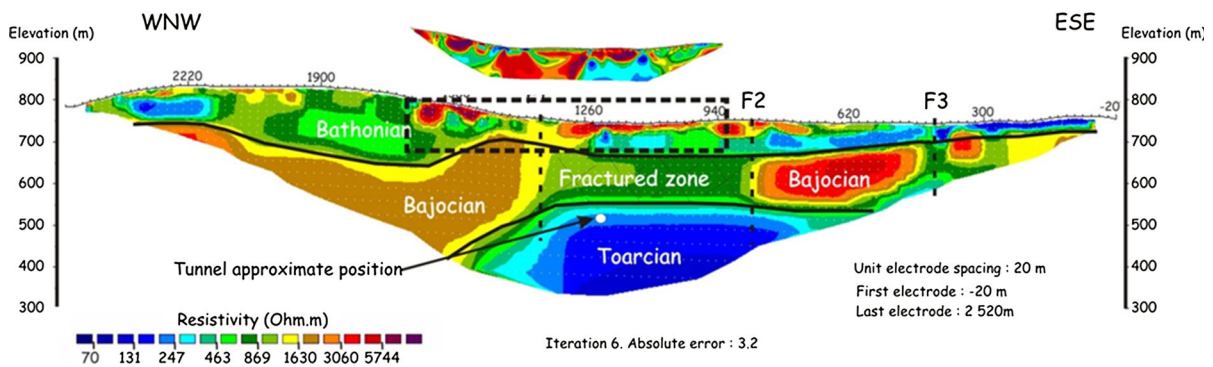

Figure 9
Comparison between the large-scale and high-resolution electrical resistivity tomography sections (Wenner array). The sections are displayed with the same color scale as Figs. 3, 4 and 8. Both sections are displayed with the same horizontal and vertical scale. The *blue line* indicates the position of the 2011 high-resolution survey

with the Schlumberger arrays and is located between 200 and 300 m lateral distance under the conductive superficial area. We could also have 2D/3D artifacts consistent between the different arrays. However, the large-scale ERT images interpretation was consistent with geological data, showing that this survey was able to capture the main features of the investigated area, even at depth. Moreover, 2D surveys are perpendicular to the fault zones at depth. These zones have a certain length (in N-S direction, see Fig. 2), which means that their possible upward continuation should also have a certain length, and therefore should appear in HR ERT images.

Some local differences appear near the surface in the higher resolution 4 and 2 m electrode spacing images in comparison with the 8 m ones. The small electrode spacing enables to better delineate thin layers (Figs. 4, 6, 7). As an example, a superficial 400–800 Ωm 5-m-thick layer appears in the 2-m electrode spacing image between 290 and 430 m in lateral distance. This thin layer with electrical resistivity about 800 Ωm is located between two layers with electrical resistivity higher than 1600 Ωm. The match between calculated and observed data for this area is very good (Fig. 5), so that the existence of this thin layer is very likely.

Moreover, the 2-m tomography section shows a lateral continuity of this thin layer, that deteriorates on its western part as electrode spacings increases and is characterized by a low-resistivity zone dipping eastward between 300 and 380 m for 4- and 8-m electrode spacing images (Fig. 4). Even if this low-resistivity zone appears in the 2-m section, it is less spatially extended in the 2-m section and is probably related to superficial electrical resistivity low values.

In an attempt to take advantage of both high resolution provided by the 4- and 2-m electrode spacing measurements and greater depth investigation provided by the 8-m electrode spacing data, we combined all data together for each array. Figure 8 shows the results of this multi-scale inversion. Electrical resistivity images obtained with the different acquisition arrays (Wenner and Schlumberger) are very similar, again indicating the stability of the results. The comparison between Figs. 4 and 8, as well as Figs. 6 and 7, shows that the multi-scale inversion allows to capture the same main low (lower than 200 Ωm) to high (higher than 5000 Ωm) electrical resistivity values. In the deeper part, electrical resistivity values correspond to the 8-m spacing whereas close to the surface, the 2-m spacing electrode acquisition provides high-resolution, allowing for example to properly detect the superficial 5-m-thick layer that appears between 290 and 430 m in lateral distance. We note that the low-resistivity zone dipping eastward between 300 and 380 m for 4- and 8-m electrode spacing images is still present.

In this section, we have compared and combined data from different arrays and electrode spacings. Before discussing the ERT images and interpreting them as soil properties, we compare in the next section high-resolution ERT results with large-scale ones.

4.2. Comparison with the 2007 Large-Scale Electrical Resistivity Profile

Figure 9 shows the comparison between the large-scale and the high-resolution ERT models plotted with the same color scale. The black-dotted rectangle on top of the large-scale ERT model roughly delineates the investigated area common to both surveys. On the whole, the same sharp-contrasted low-to-high electrical resistivity values are detected and, as expected, the high-resolution ERT images provide more details close to the surface. In particular, in both images, an electrically resistive (more than 3000 Ωm) zone between 1060 and 1260 m lateral distance on the large-scale profile overlies a conductive zone (less than 300 Ωm). Similarly, a highly resistive zone (more than 5000 Ωm) located between 1500 and 1660 m lateral distance on the large-scale profile is present on both images. Figures 10 and 11 show a quantitative comparison between large-scale and high-resolution ER values at different points along the profile. At 124, 408 and 516 m, the global trend between high-resolution and 40-m electrode spacing results is the same (Fig. 10). As expected, Fig. 11 shows that the low-resolution 40-m electrode profile is not able to quantitatively provide local small variation.

One major difference between large-scale and high-resolution ERT images can be pointed out. At the western edge of the fractured zone located at depth in Bajocian limestones and denoted as F1 on Fig. 9, electrical resistivity values are lower with the large-scale than with the high-resolution ERT images. Figure 10 shows quantitatively the difference between electrical resistivity values at 220 m. In the deeper part, electrical resistivity is lower in the low-resolution profile than in high-resolution ones. Figure 11 shows that this zone is located between 200 and 300 m.

Several reasons may explain the differences observed between large-scale and high-resolution surveys. First, the low-resolution profile may average strongly contrasted electrical resistivity values, what could explain why locally different features appear in both images. The non-uniqueness of the inversion results is likely to emphasize this. Secondly, since large-scale and high-resolution data were not acquired at the same time, the soil properties, such as water content or soil moisture, could be locally different. To limit this phenomenon, we chose to perform the high-resolution measurements in the same month (May) in order to get close weather conditions. Thirdly, the two profiles were not acquired exactly along the same line (Fig. 2). Even if the geological layers are known to be almost horizontal (5° dipping towards the north), the upper
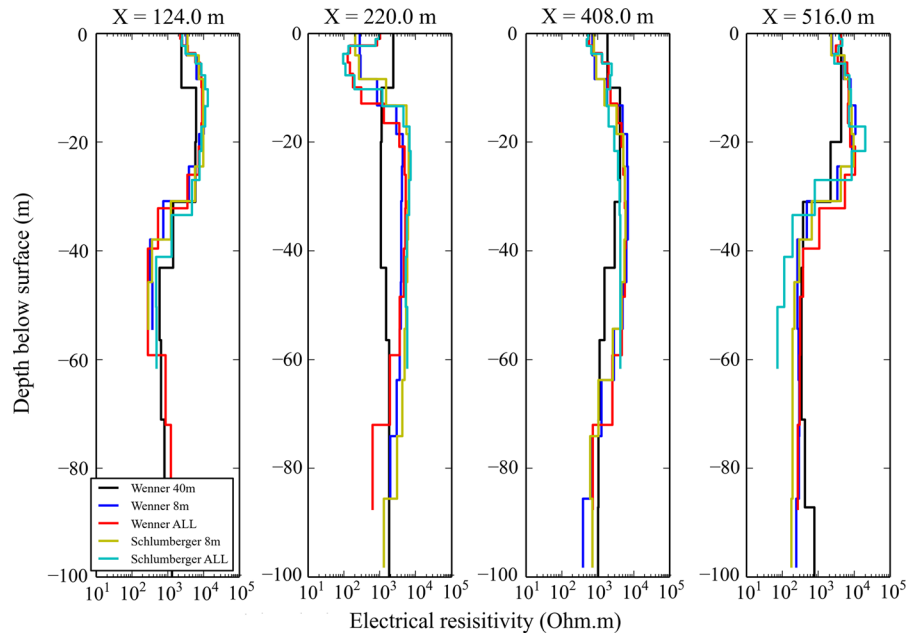
Figure 10

1D vertical electrical resistivity profiles extracted from the 8 m, combined (labeled ALL: 2, 4 and 8 m) high-resolution sections and the large-scale section (labeled 40 m). Lateral positions form *left* to *right*: 124, 220, 408 and 516 m
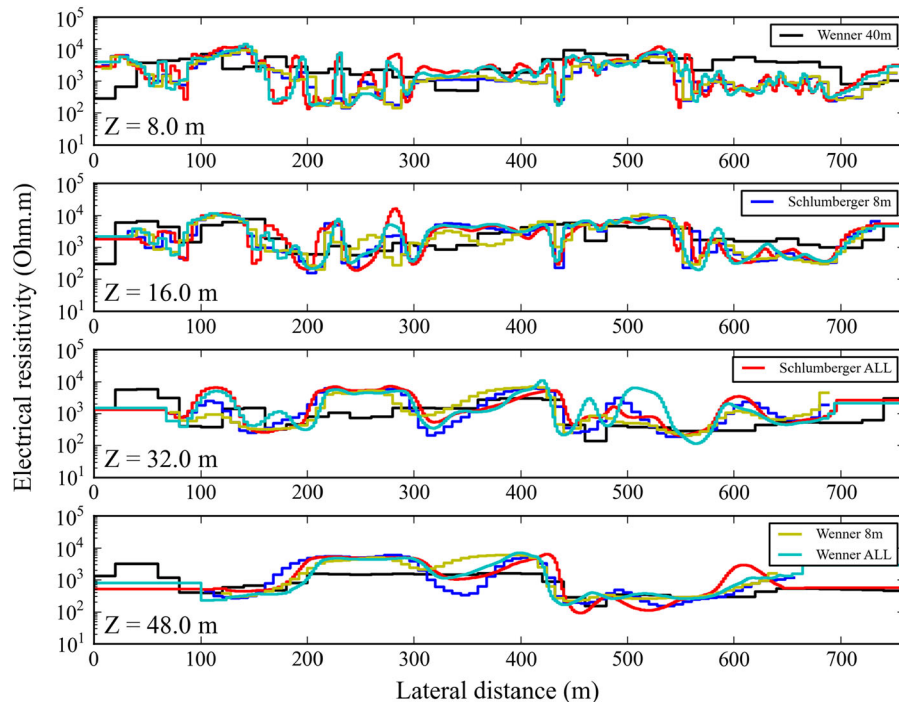

Figure 11

1D horizontal electrical resistivity profiles extracted from the 8 m, combined (labeled ALL: 2, 4 and 8 m) high-resolution sections and the large-scale section (labeled 40 m). Depth below topography from *top* to *bottom*: 8, 16, 32 and 48 m. For the high-resolution surveys electrical resistivity values on the edges are not resolved due to lack of coverage and are displayed in the graphs as constant values. This lack of coverage increases with depth. The *different colors* correspond to the different acquisitions (see *legends*)

limestones are expected to be heterogeneous, fractured and karstified. Spatial variations in this layer could be very strong in the first tens of meters. Therefore, for the last two reasons just mentioned, we could not combine together the 2007 large-scale data with the 2011 higher resolution ones to get a combined image.

In the next section, we try to assess the potential and limitations of our electrical resistivity images through a comparison with field observations.

5. Interpretation of Electrical Resistivity Images and Comparison with Geological Data

We compare in this section the Schlumberger inversion results combining all electrode spacings with a geological cross-section. We only concentrate on one of the combined inversion result as both arrays Wenner and Schlumberger give similar results (Fig. 8).

Figure 12 (top) shows the geological cross-section obtained from a field observations, from the known stratigraphic sequence, from the interpretation of aerial pictures and from the prolongation of known fault zones recognized on the cliffs located south of the ERT profiles (see Figs. 1, 2). This geological cross-section is therefore based on data independent from the ERT results. For reference and comparison the Schlumberger section combining all electrode spacing data is displayed below and finally both sections are superimposed in Fig. 13.

The geological cross-section shows that subsurface layers are subhorizontal. They are mainly composed of limestones and dolomites. Some sandy or argillaceous layers are present as well. ERT images show strong lateral resistivity variations (Figs. 4, 5, 6, 7, 8, 9, 10, 11), located inside the same geological layer. These variations are probably due to faults and fractured zones that could lead to preferential erosion and to water circulation along these discontinuities. Based on similar ER values and structure, we divide the ERT image into different parts (Fig. 13). In the following we interpret these parts with the help of the geological cross-section (Fig. 13).

At the western part, between 0 and 200 m lateral distance (part a in Fig. 13), alternative superficial low and high ER values are associated to the presence of weathered and locally fractured limestones. At depth, a more conductive zone (ER values lower than 800 Ωm under ER values higher than 4000 Ωm) is present. However, the top of this zone is not subhorizontal in ERT images (although it is more horizontal with the Wenner acquisition geometry, more sensitive to horizontal layering), whereas the geological cross-section indicates that layers are subhorizontal. As already mentioned, this is mainly interpreted as the presence of fractures in a chaotic dolomitic zone. This may be as well due to some artifacts in the ER data inversion due to the topography (PENZ et al. 2013). At 50 and 88 m lateral distance, local ER lower values correspond to faults visible in the field. At around 190 m lateral distance, a sharp contrast (ER values from 800 to 4000 Ωm) is present at depth. It is correlated to the presence of a fault in this area that may cross the whole geological series.

At the eastern part of the profile (lateral distance higher than 580 m, part g in Fig. 13), limestone is characterized by heterogeneous ER values and low values correspond to the presence of faults and fractures.

Then, between 200 and 300 m lateral distance (part b in Fig. 13), a zone dominated by two superficial strongly conductive layers (ER lower than 400 Ωm at around 220 and 284 m) is located above a highly resistive layer (higher than 3000 Ωm). The resistive layer corresponds to Bathonian limestones and the conductive zone may be interpreted as an area of superficial water runoff. Zones with the lowest ER values are roughly consistent with the presence of identified faults at the surface. The overall electrical resistivity values of this zone are different from the ones obtained with the low-resolution profile (Figs. 2, 9, 10). As already discussed, this may be related to the different resolutions of both images. The low-resolution profile may average strongly contrasted electrical resistivity values.

Another zone (300–430 m lateral distance, part c in Fig. 13) is characterized by a shallow low ER layer (400–800 Ωm) imbedded between two more resistive layers (higher than 1600 Ωm). The resistive layers
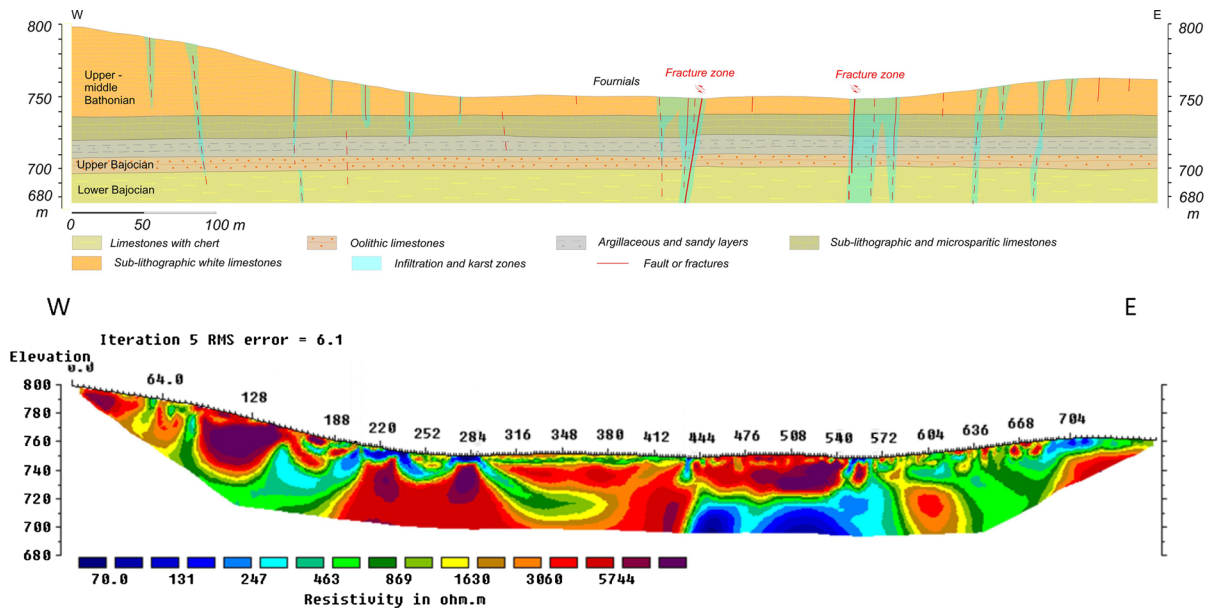
Figure 12
Geological cross-section (*top*) showing the subhorizontal layering along with the subvertical faults and fracture zones marked in *red* and Schlumberger section combining all electrode spacing data (*bottom*) for reference and comparison. Infiltration zones and karsts are displayed in *light blue* in the top figure
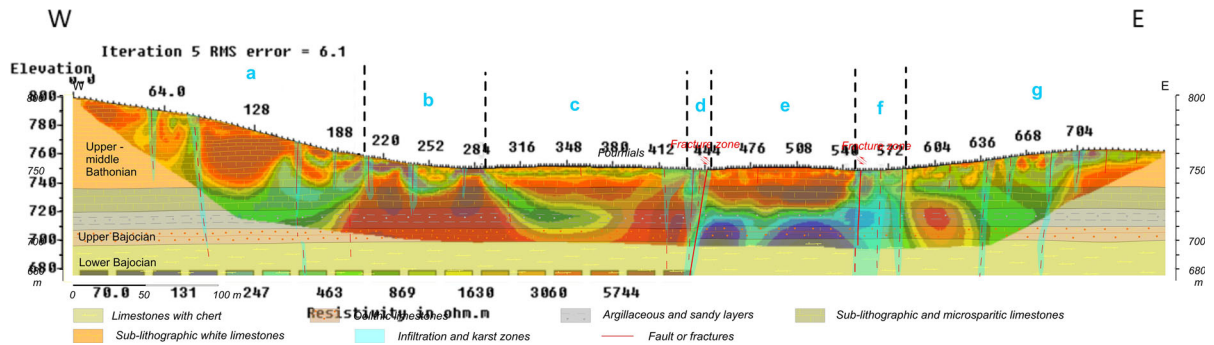

Figure 13
Geological cross-section superimposed on the Schlumberger electrical resistivity section (Fig. 12)

are interpreted as limestones while the more conductive zone is associated to a thin layer (few meters thick) composed of an intercalation of limestone, sandy and argillaceous layers. At depth, a low-resistivity zone (ER values lower than 800 Ωm) dipping eastward between 300 and 380 m ER zone appears. It is very likely to be an artifact produced by the inversion due to a very shallow strong contrast at 284 m. NGUYEN *et al.* (2007) studied and showed similar inversion artifacts due to this kind of near subsurface heterogeneities. However, it might

correspond to the presence of a fault zone at depth (dotted line in the geological cross-section) whose presence was inferred from the prolongation towards the northwest direction of a fault zone identified in the cliffs under the surface of the plateau.

The zone between 440 and 540 m lateral distance (part e in Fig. 13) is composed of two main layers: in the shallow one, ER values are above 3000 Ωm, whereas in the deep layer ER values are below 350 Ωm. The shallow layer corresponds to a limestone layer; its nearly horizontal basis can be

associated to the top of an argillaceous and sandy sedimentary subhorizontal layer as shown in the geological cross-section.

The two subvertical conductive corridors that reach the surface (430–440 m and 540–580 m in lateral distance, parts d and f in Fig. 13) correspond to fractured zones inferred from geological data and can be correlated with similar observations in the underground works (Fig. 4). These two corridors also correspond to the lateral limit of the conductive zone located in depth between 440 and 540 m on the same line. This is interpreted as the presence of fractured zones reaching the sandy and argillaceous layer. This may correspond to the presence of water in this argillaceous and sandy layer, guided and restricted between two fault zones.

6. Discussion and Conclusion

In this study, we assessed the potential of Electrical Resistivity tomography surveys to image fault and fractured zones in the Experimental Platform of Tournemire. We first compare ERT images acquired with the Wenner configuration and electrode spacing ranging from 2 to 40-m. High-resolution acquisitions allow to investigate the first hundred meters in depth in more detail than the large-scale survey does. We find an overall good agreement between results, in particular for results acquired at the same period (electrode spacing 2, 4 and 8 m). This leads us to invert simultaneously data acquired with these different spacings. This multi-resolution approach allows a greater investigation in depth (with the 8-m electrode spacing) and the higher resolution in the near subsurface (with the 2-m electrode spacing). Images obtained with both arrays (Wenner and Schlumberger) are in good agreement.

To quantitatively assess the level of similarity of results obtained with different configurations and electrode spacing, we compare 1D profiles (vertical and horizontal) for the 2, 4, 8 m and the multi-scale inversion extract from the ERT images. Similar comparison is shown for the 8, 40 m and multi-scale results. The interpretation of the 2D color ERT images alone can be fairly difficult, the 1D profiles allow a better delineation between the different

reconstructed resistivity parts; Nguyen et al. (2005) with a different data set came to the same conclusion and showed similar figures.

To evaluate the quality of the ERT images beyond the unique RMS value, we superimpose observed and computed apparent resistivity data, that allows to potentially identify poorly resolved areas in the sections. In our case, computed data fit observations very well, this only means that the ERT sections we obtained can explain the recorded data. As pointed out by Nguyen et al. (2005) and many other authors, this does not guarantee that the results we obtained correspond to reality and many different models can equivalently explain the data. Therefore, we only focused on the electrical resistivity contrasts in the images for their interpretation.

To interpret electrical resistivity contrasts, we compare them with a geological cross-section build from independent data. As noticed by Nguyen et al. (2007), this is of first importance to interpreting ERT profiles. On the whole, subvertical conductive zones in ERT images are in agreement with fault zones identified in the geological cross-section. The top of a more conductive zone, below a high electrical conductive zone and between two subvertical fault zones, is interpreted as the presence of a more scattered fracture zone located at depth between two fault zones. These zones location could be correlated with the fractured zones identified at 250-m depth in underground works.

Interpretation of ERT results is more delicate when differences appear between results obtained with different configurations or scales. As an example, in our study, the main difference between large-scale (40-m) and high-resolution (8-m and less) results concerns a zone located at the bottom of the small hill in the west part of the profile. This area appears to be more conductive in the large-scale image than in the high-resolution profile and is constant from top to bottom in the large-scale image, whereas it is composed of one highly conductive superficial zone overlaying a resistive zone in the high-resolution images. This may be related to the different resolutions of both images. The low-resolution profile may average strongly contrasted electrical resistivity values. Another interpretation could be to consider a conductive zone dipping from

this area in some images. It might correspond to the presence of a fault zone at depth, indicated on the geological cross-section, whose presence was inferred from the prolongation towards the northwest direction of a fault zone identified in the cliffs under the surface of the plateau. We consider as most likely the interpretation of this dipping conductive zone as an inversion artifact. This is supported by lower relative sensitivity values at depth below conductive superficial zone between 200 and 300 lateral distance with Schlumberger arrays, suggesting that ERT images are less reliable in this part. However, in this case, the geological cross-section does not allow us to unambiguously choose between the two possible interpretations.

This study shows the potential of ERT surveys to detect fault and fractured zones in near subsurface layers. This clearly highlights the interest of using multi-scale acquisitions, that takes benefit from small take-outs, allowing to finely image the soil electrical resistivity properties, and larger take-outs, allowing to image deeper soil structures.

We plan to perform such a feasibility study with some high-resolution seismic data acquired in the Experimental Station of Tournemire (e.g., VI NHU BA et al. 2013), allowing to assess the ability of seismic data to detect fault and fracture zones. Should the results be convincing, we could combine together high-resolution electrical resistivity and seismic data. Such studies could help in particular to choose between the interpretations proposed by large-scale and high-resolution electrical resistivity images at the bottom of the small hill in the western part of the profile.

Acknowledgments

REFERENCES

BINLEY, A. and KEMNA, A. Dc resistivity and induced polarization methods. In: Hydrogeophysics. Springer; 2005. p. 129–156.

BOISSON, J., BERTRAND, L., HEITZ, J. and GOLVAN, Y. (2001). *In-situ and laboratory investigations of fluid flow through an argillaceous formation at different scales of space and time, Tournemire tunnel, Southern France.* Hydrogeology Journal 9, 108–123.

BOISSON, J., CABRERA, J. and de WINDT, L. (1996). Investigation faults and fractures in an argillaceous formation at the IPSN Tournemire research site. In: Proc. OECD/NEA-E.C. International Workshop on Fluid Flow Through Faults and Fractures in Argillaceous Formation, Berne, 10–12 June

BONIN, B. (1998). *Deep geological disposal in argillaceous formations: studies at the Tournemire test site.* Journal of Contaminant Hydrology 35, 315–330.

CABRERA, J., BEAUCAIRE, C., BRUNO, G., de WINDT, L., GENTY, A., RAMAMBASOA, N., REJEB, A., SAVOYE, S. and VOLANT, P. (2001). Projet Tournemire: synthèse des résultats des programmes de recherche 1995/1999. In: IRSN report.

CAPUTO, R., PISCITELLI, S., OLIVETO, A., RIZZO, E. and LAPENNA, V. (2003). *The use of electrical resistivity tomographies in active tectonics: examples from the Tyrnavos Basin, Greece.* J. Geodyn. 36, 19–35.

COSENZA, P., GHORBANI, A., FLORSCH, N. and REVIL, A. (2007). *Effects of drying on the low-frequency electrical properties of Tournemire argilites.* P. Appl. Geophys. 164, 2043–2066.

DAHLIN, T. and LOKE, M. (1998). *Resolution of 2D Wenner resistivity imaging as assessed by numerical modelling.* J. App. Geophys. 38, 237–249.

DAHLIN, T. and ZHOU, B. (2004). *A numerical comparison of 2D resistivity imaging with 10 electrode arrays.* Geophys. Prospect. 52, 379–398.

DEMANET, D., PIRARD, E., RENARDY, F. and JONGMANS, D. (2001). *Application and processing of geophysical images for mapping faults.* Computers and Geoscience 27, 1031–1037.

FRID, V., LISKEVICH, G., DOUDKINSKI, D. and KOROSTISHEVSKY, N. (2008). *Evaluation of landfill disposal boundary by means of electrical resistivity imaging.* Environmental Geology 53, 1503–1508.

GÉLIS C., REVIL A., CUSHING M. E., JOUGNOT D., LEMEILLE F., CABRERA J., De HOYOS A., ROCHER M. (2010). *Potential of Electrical Resistivity Tomography to Detect Fault Zones in Limestone and Argillaceous Formations in the Experimental Platform of Tournemire, France.* P. Appl. Geophys, vol. 167, no. 11, pp. 1405–1418,

GIBERT, D., NICOLLIN, F., KERGOSIEN, B., BOSSART, P., NUSSBAUM, C., GRISLIN-MOUËZY, A., CONIL, F., HOTEIT, N., 2006. *Electrical tomography monitoring of the excavation damaged zone of the gallery 04 in the Mont Terri rock laboratory: Field experiments, modelling, and relationship with structural geology.* Applied clay science; 33 (1) : 21–34.

GRANDJEAN G., HIBERT C., MATHIEU F., GAREL E. and MALET J.-F., 2009. *Monitoring water-flow in a clay-shale hillslope from geophysical data fusion based on a fuzzy logic approach.* C. R. Gesciences 341, 937–948.

GUÉRIN, R., MUNOZ, M., ARAN, C., LAPERRELLE, C., HIDRA, M., DROUART, E. and GRELLIER, S. (2004). *Leachate recirculation: moisture content assessment by means of a geophysical technique.* Waste Management 24, 785–794.

HAMZAH, U., YAACUP, R., SAMSUDIN, A. and AYUB, M. (2006). *Electrical imaging of the groundwater aquifer at Banting, Selangor, Malaysia.* Environmental Geology 49, 1156–1162.

IMPROTA L., FERRANTI L., DE MARTINI P.M., PISCITELLI S., BRUNO P.P., BURRATO P., CIVICO R., GIOCOLI A., IORIO M., D'ADDEZIO G.

and MASCHIO L., 2010. *Detecting young, slow-slipping active faults by geologic and multi-disciplinary high-resolution geophysical investigations : a case study for the Apennine seismic belt, Italy*. J. Geophys. Res., *115*, B11307.

KRUSCHWITZ, S. and YARAMANCI, U., 2004. *Detection and characterization of the disturbed rock zone in claystone with complex resistivity method*. Journal of Applied Geophysics 57, 63–79.

LEROY, P., REVIL, A., ALTMANN, S. and TOURNASSAT, C. (2007). *Modeling the composition of the pore water in a clay-rock geological formation (Callovo-Oxfordian, France)*. Geochimica et Cosmochimica Acta 71 (5), 1087–1097.

LOKE, M. and BARKER, R. (1995). *Least-squares deconvolution of apparent resistivity pseudosections*. Geophysics 60 (6), 1682–1690.

LOKE, M. and BARKER, R. (1996). *Rapid least-squares inversion of apparent resistivity pseudosections by a quasi-Newton method*. Geophysical Prospecting *44*, 131– 152.

MERIC, O., GARAMBOIS, S., JONGMANS, D., WATHELET, M., CHATELAIN, J. and VENGEON, J. (2005). *Application of geophysical methods for the investigation of the large gravitational mass movement of Séchilienne, France*. Can. Geotech. Journal *42*, 1105–1115.

NGUYEN F., S. GARAMBOIS, D. CHARDON, D. HERMITTE, O. BELLIER and D. JONGMANS (2007). *Subsurface electrical imaging of anisotropic formations affected by a slow active reverse fault, Provence, France*. Journal of Applied Geophysics 62, 338–353.

NGUYEN F., GARAMBOIS S., JONGMANS D., PIRARD E. and LOKE M.H. (2005). *Image processing of 2D resistivity data for imaging faults*. Journal of Applied Geophysics, 57, 260-277.

PENZ S., CHAURIS H., DONNO D. and MEHL C. (2013). *Resistivity modelling with topography*. Geophys. J. Int., *194*, 1486–1497

REVIL, A., FINIZOLA, A., PISCITELLI, A., RIZZO, E., RICCI, T., CRESPY, A., ANGELETTI, B., BALASCO, M., BARDE CABUSSON, S., BENNATI, L., BOLÈVE, A., BYRDINA, S., CARZANIGA, N., DI GANGI, F., MORIN, J., PERRONE, A., ROSSI, M., ROULLEAU, E. and SUSKI, B. (2008). *Inner structure of la Fossa di vulcano (vulcano island, southern Tyrrhenian Sea, Italy) revealed by high resolution electric resistivity tomography coupled with self-potential, temperature, and soil CO2 diffuse degassing measurements*. Journal of Geophysical Research, *113*, B07207, doi:10.1029/2007JB005394.

RIZZO, E., COLELLA, A., LAPENNA, V. and PISCITELLI, S. (2004). *High-resolution images of the fault-controlled high Agri valley basin (Southern Italy) with deep and shallow resistivity tomographies*. Physics and Chemistry of the Earth 29, 321–327.

ROBERT T., DASSARGUES A., BROUYÈRE S., KAUFMANN O., HALLET V. and NGUYEN F., 2011. *Assessing the contribution of electrical resistivity tomography (ERT) and self-potential (SP) methods for a water well drilling program in fractured/karstified limestones*. Journal of Applied Geophysics 75, 42–53

STORZ, H., STORZ, W. and JACOBS, F. (2000). *Electrical resistivity tomography to investigate geological structures of the earth's upper crust*. Geophysical Prospecting *48* (3), 455–471.

SUZUKI, K., TODA, S., KUSUNOKI, K., FUJIMITSU, Y., MOGI T., and JOMORI, A. (2000). *Case studies of electrical and electromagnetic methods applied to mapping active faults beneath the thick quaternary*. Engineering Geology 56, 29–45.

TROUILLER, A. (2006). *The Callovo-Oxfordian of the Paris basin: from its geological context to the modelling of its properties*. Comptes Rendus Geosciences, *338*, 815–823.

VANNESTE, K., VERBEECK, K. and PETERMANS, T. (2008). *Pseudo-3D imaging of low-slip-rate, active normal fault using shallow geophysical methods: The Geleen fault in the Belgian Maas river valley*. Geophysics *73* (1), B1–B9.

VI NHU BA, E., NOBLE, M., GÉLIS, C., GESRET, A., & CABRERA, J. (2013). *Geophysical imaging of near subsurface layers to detect fault and fractured zones in the Tournemire experimental Platform, France.*, in EGU General Assembly Conference Abstracts, vol. 15, p. 7783.

YVEN, B., SAMMARTINO, S., GÉRAUD, Y., HOMAND and F. VILLIÉRAS (2007). *Mineralogy, texture and porosity of Callovo-Oxfordian argillites of the Meuse/Haute-Marne region (eastern Paris basin).* Bulletin de la Société Géologique de France *178*, 73–90